Acoustic wave reflection by stellar cores: can it be seen in the autocorrelation function of p-mode measurements?

Ian W. Roxburgh, Sergei Vorontsov

Mon. Not. R. Astron. Soc. **379,** 801–806 (2007) doi:10.1111/j.1365-2966.2007.11979.x

Acoustic wave reflection by stellar cores: can it be seen in the autocorrelation function of p-mode measurements?

I. W. Roxburgh[1,2⋆] and S. V. Vorontsov[1,3]

[1]*Astronomy Unit, Queen Mary, University of London, Mile End Road, London E1 4NS*
[2]*LESIA, Observatoire de Paris, Place Jules Janssen, 92195 Meudon, France*
[3]*Institute of Physics of the Earth, B. Gruzinskaya 10, Moscow 123810, Russia*

Accepted 2007 May 10. Received 2007 March 26

ABSTRACT

The rapid variation of density with depth in a stellar core can distort acoustic wave propagation in stellar interiors, producing a reflected wave. The reflectivity can come from a rapid density change at the boundary of a convective core, or from the steep gradients established in a radiative core during chemical evolution. We analyse this wave reflection within the framework of wave scattering theory, and address the question of the detectability of the reflected wave in the autocorrelation function of stellar p-mode measurements.

Key words: methods: numerical – stars: oscillations.

1 INTRODUCTION

In solar-like stars, multiple p modes are expected to be stochastically excited by random events associated with convective motion near the stellar surface. An obvious way of sounding stellar interiors thus consists of measuring and further analysing stellar p-mode frequencies. The accurate measurement of multiple p-mode frequencies is not a simple task, however, principally due to the small amplitudes of the stochastically driven oscillations. It is thus desirable to develop alternative means of data analysis, which would circumvent direct frequency measurements.

Such an alternative diagnostic tool is the analysis of the autocorrelation function (ACF) of the observational time string of variations in intensity or Doppler velocity. The ACF represents an integral transform (Fourier transform) of the power spectrum, capable of capturing particular features of collective p-mode behaviour in noisy data. The first and obvious implementation is the measurement of stellar acoustic diameter (or, equivalently, the 'large frequency separations') by determining the position of the dominant peak in the ACF. The ACF can also be used to estimate the 'small frequency separations' from rather poor data (Roxburgh & Vorontsov 2006, hereafter Paper I).

In theoretical investigations, a simple but powerful tool for analysing the propagation in stellar interiors of acoustic waves modified by buoyancy and gravity is provided by the semiclassical (short-wave) approximation (Roxburgh & Vorontsov 2000a,b). In this approximation, the waves propagate like particles along well-defined rays. The ray trajectories, which account for the slowly varying refractive properties in the media, are governed largely not only by the sound-speed profile, but also by buoyancy and gravity perturbations. For a downward ray, buoyancy has an effect similar to the increase of the sound speed, which deflects the ray away from the stellar centre (repulsive interaction). Gravity has the opposite effect (attractive interaction). It is the delicate balance between these effects (all of which are significant in stellar cores) which governs the forward amplitude (the wave amplitude at a point on the surface opposite to the source). The 'small frequency separation' is just a quantity inversely proportional to the forward amplitude.

In this paper, we consider the situation when the classical picture of wave propagation is destroyed. The perturbing agent is the stellar core, where the applicability of semiclassical analysis can be violated by the rapid variation of seismic parameters with depth (on a scale less than acoustic wavelength), which will create a reflected wave. The influence of rapid spatial variations on p-mode frequencies and on frequency separations was analysed earlier (e.g. Roxburgh & Vorontsov 2001, and references therein) in the framework of solutions to the oscillation equations. Here, we analyse the perturbation of the acoustic wave field and address the detectability of the wave reflection in the ACF.

2 MONOCHROMATIC WAVE FIELD

In Section 2.1, we recall the results of Roxburgh & Vorontsov (2000a), which will be used as our starting point, and express them in a form convenient for subsequent analysis (equations 10–12).

2.1 Semiclassical wave propagation

In the analysis of a global wave field, we consider its behaviour in a thin spherical layer with thickness of the order of the local acoustic wavelength. The layer is positioned somewhere in the stellar envelope, but not too far from the surface for the acoustic waves, which constitute the low-degree p modes, to be nearly vertical. We assume

⋆E-mail: I.W.Roxburgh@qmul.ac.uk

that in this layer the Cowling approximation is applicable, buoyancy effects are small and the sound speed $c(r)$ is a smooth function of radial coordinate r; the wave equations then reduce to the simple form as

$$\nabla^2\psi + k^2(r)\psi = -\delta\left(\boldsymbol{r} - \boldsymbol{r}_{\rm s}\right), \tag{1}$$

where $\psi(\boldsymbol{r}) = \rho_0^{-1/2}\ (r)p'(\boldsymbol{r})$, $k^2(r) = \omega^2/c^2(r)$, $p'(\boldsymbol{r})$ is the Eulerian pressure perturbation and the time dependence is separated as $\exp(-{\rm i}\omega t)$. From now on, time will not enter the equations, and we will use t to designate the acoustic radius $t = \int_0^r {\rm d}r/c$. We consider an artificial point-like harmonic excitation source to be positioned at $\boldsymbol{r} = \boldsymbol{r}_{\rm s}$ within the layer and analyse the wave field $\psi(\boldsymbol{r})$ created by this source, imposing free outgoing-wave boundary conditions above $r = r_{\rm s}$ to eliminate the surface reflection. The wave field is decomposed in spherical harmonics as

$$\psi(\boldsymbol{r}) = \sum_{l=0}^{\infty} \frac{c^{1/2}(r)}{r}\psi_l(r)Y_{l0}(\theta,\phi) \tag{2}$$

in a coordinate system, where the source is located at $\theta = \pi$. The wave field is also represented as

$$\psi(\boldsymbol{r}) = A(\boldsymbol{r}){\rm e}^{{\rm i}S(\boldsymbol{r})} \tag{3}$$

with real amplitude A and real action S. In the classical limit, S is large quantity.

It is shown in Roxburgh & Vorontsov (2000a) that in the conditions when wave propagation is nearly classical everywhere below the layer, including the stellar core, the radial functions of partial waves $\psi_l(r)$ behave in the vicinity of $r = r_{\rm s}$ (but slightly below $r_{\rm s}$) as

$$\psi_l(r) = A_l\left(r_{\rm s}\right)\sin\left(\omega t - \frac{\pi}{2}\,l + \delta_l\right), \tag{4}$$

where t is acoustic radius defined above and the phase shifts δ_l depend on l at low degree l as

$$\delta_l = \delta_0 + l(l+1)D_\delta. \tag{5}$$

This leads to the eigenfrequency equation of low-degree modes

$$\omega T + \delta_0(\omega) + l(l+1)D_\delta(\omega) \simeq \pi\left[n + \frac{l}{2} + \frac{1}{4} + \alpha_{\rm out}(\omega)\right], \tag{6}$$

where T is the stellar acoustic radius, n the radial order and $\alpha_{\rm out}$ a surface phase shift. The parameter D_δ in equations (5) and (6) is a quantity which governs the small frequency separations:

$$D_\delta = \frac{1}{4}\left(\frac{\partial S}{\partial z}\right)^{-1}_{r_{\rm s},1} = \frac{1}{16\pi r_{\rm s}^2 k_{\rm s} A\left(r_{\rm s},1\right)}, \tag{7}$$

where the action S and the amplitude A are the functions of r and $z = \cos(\theta)$, so that $A(r_{\rm s}, 1)$ is forward amplitude and $k_{\rm s} = k(r_{\rm s})$. In equation (4), the amplitudes of low-degree partial waves are

$$A_l\left(r_{\rm s}\right) = \frac{c^{-1/2}(r_{\rm s})}{r_{\rm s}k_{\rm s}}\left(\frac{2l+1}{4\pi}\right)^{1/2}\exp\left[{\rm i}\left(\omega t_{\rm s} + \frac{\pi}{2}\,l + \delta_l\right)\right], \tag{8}$$

with $t_{\rm s} = t(r_{\rm s})$.

It will be productive for further analysis to replace the decomposition of the wave field $\psi(\boldsymbol{r})$ into partial waves (standing waves) by an equivalent decomposition into travelling waves. Using the identity

$$\sin\left(x - \frac{\pi}{2}\,l\right) = \frac{1}{2{\rm i}}\left[(-i)^l{\rm e}^{{\rm i}x} - i^l{\rm e}^{-{\rm i}x}\right], \tag{9}$$

it is straightforward to show that the spherical harmonic expansion specified by equations (2), (4) and (8) is equivalent to

$$\psi(\boldsymbol{r}) = \sum_{l=0}^{\infty}\psi_l(r,\theta), \tag{10}$$

where (at low-degree l)

$$\psi_l(r,\theta) = \frac{2l+1}{8\pi i r_{\rm s}^2 k_{\rm s}}P_l(\cos\theta) \times\left[(-1)^{l+1}{\rm e}^{-{\rm i}k_{\rm s}(r-r_{\rm s})} + S_l{\rm e}^{{\rm i}k_{\rm s}(r-r_{\rm s})}\right], \tag{11}$$

with Legendre polynomials $P_l(\cos\theta)$ and with

$$S_l = {\rm e}^{2{\rm i}(\omega t_{\rm s} + \delta_l)}. \tag{12}$$

There should be no confusion between $\psi_l(r,\theta)$, now a function of two variables, and $\psi_l(r)$ in equations (2) and (4).

The reader might now note more similarities between the spherical harmonic expansion (10)–(12) and corresponding expansions of the wave field which are commonly used in quantum scattering theory (Landau & Lifshitz 1976). The major difference is that in our problem, the wave source is located at a finite distance from the scatterer and is embedded in the refracting medium.

2.2 Wave scattering by a stellar core

The results listed above were obtained under the assumption that wave propagation is nearly classical in the deep stellar interior, which allowed us to obtain equation (5) for the phase shifts. If we are not concerned with the particular properties of the phase shifts, but just define them as phases of partial waves in the vicinity of $r = r_{\rm s}$ (equation 4), the spherical harmonic expansions (2, 4 and 8) and (10–12) are more generally valid, independent on any assumptions about wave propagation in the interior except that of spherical symmetry of the media and that there are no energy losses.

Now suppose that the stellar core, of acoustic radius small compared to $t_{\rm s}$ so that the core structure only influences the low-degree components in the expansion, is modified in an arbitrary manner. For the acoustic field outside the core, this modification is described uniquely by the replacement of the phase shifts δ_l with their new values $\delta_l + \Delta\delta_l$. Modification of the l-component of the wave field (equation 11) comes through the variation of S_l defined by equation (12). Assuming $\Delta\delta_l$ to be small, we get

$$\Delta\psi_l(r,\theta) = \frac{(2l+1)\Delta\delta_l}{4\pi r_{\rm s}^2 k_{\rm s}}P_l(\cos\theta)S_l{\rm e}^{{\rm i}k_{\rm s}(r-r_{\rm s})}. \tag{13}$$

If the modification of the core produces wave reflection, it is this signal from which the reflectivity can be measured. We note, however, that scattering does not necessary mean reflection. The core can well be modified in a way which keeps it 'transparent' to acoustic waves, so that it is only the refractive properties of the media which change without producing any reflected wave. To make a distinction, we need to involve an observer.

2.3 Signals detected by an 'observer'

We assume that observations are performed from a large distance, with sensitivity across the stellar disc specified by function $s(\theta)$ for an observer located at $\theta = 0$. As in Paper I, we introduce sensitivity coefficients c_l through the expansion

$$s(\theta) = \sum_l c_l Y_{l0}(\theta,\phi), \tag{14}$$

$$c_l = \pi^{1/2}(2l+1)^{1/2}\int_0^\pi s(\theta)P_l(\cos\theta)\sin\theta\,\mathrm{d}\theta. \quad (15)$$

Since the spherical harmonics are normalized, we have

$$\sum_l c_l^2 = 2\pi\int_0^\pi s^2(\theta)\sin\theta\,\mathrm{d}\theta. \quad (16)$$

Since $s(\theta)$ is zero at $\theta > \pi/2$, we have another useful property (Paper I)

$$\sum_l (-1)^l c_l^2 = 0. \quad (17)$$

In this paper, we will need some further properties of the sensitivity coefficients which we now derive. Written in terms of Legendre polynomials equation (14) is

$$s(\theta) = \sum_l \left(\frac{2l+1}{4\pi}\right)^{1/2} c_l P_l(\cos\theta). \quad (18)$$

On setting $\theta = 0$, we get the sensitivity at the disc centre

$$s(0) = \sum_l \left(\frac{2l+1}{4\pi}\right)^{1/2} c_l, \quad (19)$$

since $P_l(1) = 1$. On setting $\theta = \pi$, we get

$$\sum_l (-1)^l (2l+1)^{1/2} c_l = 0, \quad (20)$$

since $P_l(-1) = (-1)^l$. Differentiating both the sides of equation (18) with respect to $z = \cos\theta$ at $z = -1$, we get

$$\sum_l (-1)^l l(l+1)(2l+1)^{1/2} c_l = 0, \quad (21)$$

since $\mathrm{d}P_l(z)/\mathrm{d}z = (-1)^{l+1}\, l(l+1)/2$ at $z = -1$.

Observer 1. We place the observer at $\theta = \pi$ (the source side), and assume that what they observe is the variation of the wave field $\Delta\psi$ specified by $\Delta\psi_l$ (equation 13) at $r = r_\mathrm{s}$. The signal which is detected is

$$O_1 = 2\pi\int_0^\pi \Delta\psi(r_\mathrm{s},\theta)s(\theta)\sin\theta\,\mathrm{d}\theta, \quad (22)$$

where $\Delta\psi$ is now viewed in the coordinate system of the observer. We substitute $\Delta\psi_l$ from equation (13) with P_l replaced by $(-1)^l P_l$ to account for the translation of the coordinate system, take the components of the sensitivity function from equation (18) and sum over l to get

$$O_1 = \frac{1}{r_\mathrm{s}^2 k_\mathrm{s}}\sum_l \Delta\delta_l(-1)^l\left(\frac{2l+1}{4\pi}\right)^{1/2} c_l S_l. \quad (23)$$

To stay in the leading-order approximation of semiclassical analysis (which is always applied in the envelope), we will discard the degree-dependence of S_l in this expression (since D_δ is small at large k_s, see equations 5, 7 and 12). The result then simplifies to

$$O_1 = \frac{1}{r_\mathrm{s}^2 k_\mathrm{s}}\mathrm{e}^{2\mathrm{i}(\omega t_\mathrm{s}+\delta_0)}\sum_l \Delta\delta_l(-1)^l\left(\frac{2l+1}{4\pi}\right)^{1/2} c_l. \quad (24)$$

Suppose that in the initial configuration (before the modification), the core was transparent to acoustic waves (semiclassical wave propagation). Using properties of the sensitivity coefficients (equations 20 and 21), we conclude that the observer will see no reflection if $\Delta\delta_l$ depends on l as a linear function of $l(l+1)$. In other words, any modification of the stellar core which keeps the phase shifts in agreement with semiclassical relation (5) does not produce any reflection, but only changes δ_0 and D_δ (which describe the refractive properties of the media), a result which was to be expected.

Observer 2. We place this observer at $\theta = 0$ (the far side) to measure the direct wave refracted by the core (semiclassical wave propagation). The signal is evaluated as

$$O_2 = 2\pi\int_0^\pi \psi(r_\mathrm{s},\theta)s(\theta)\sin\theta\,\mathrm{d}\theta \quad (25)$$

with ψ specified by expansion (10)–(12). Terms with $(-1)^{l+1}$ drop from the result due to equation (20). Discarding again the dependence of S_l on degree l and using equation (19), we arrive at

$$O_2 = \frac{s(0)}{2\mathrm{i}r_\mathrm{s}^2 k_\mathrm{s}}\mathrm{e}^{2\mathrm{i}(\omega t_\mathrm{s}+\delta_0)}. \quad (26)$$

It is instructive to evaluate the same signal by direct integration of the wave field in angular coordinates without using its spherical harmonic expansion. In the hemisphere which is 'visible' to the observer, the action S in equation (3) is a rapidly varying function of θ, with one stationary point at $\theta = 0$. We substitute the expression (3) into equation (25) and replace S temporarily with λS to evaluate the integral in the classical limit (large S). Using $z = \cos\theta$ as the independent variable,

$$\begin{aligned} O_2 &= 2\pi\int_0^1 s(\theta(z))A(r_\mathrm{s},z)\mathrm{e}^{\mathrm{i}\lambda S(r_\mathrm{s},z)}\,\mathrm{d}z \\ &= \frac{2\pi}{\mathrm{i}\lambda}\int_0^1 sA\left(\frac{\partial S}{\partial z}\right)^{-1}\frac{\mathrm{d}}{\mathrm{d}z}\left(\mathrm{e}^{\mathrm{i}\lambda S}\right)\mathrm{d}z \\ &= \frac{2\pi}{\mathrm{i}\lambda}s(0)A(r_\mathrm{s},1)\left(\frac{\partial S}{\partial z}\right)^{-1}_{r_\mathrm{s},1}\mathrm{e}^{\mathrm{i}\lambda S(r_\mathrm{s},1)} \\ &\quad - \frac{2\pi}{\mathrm{i}\lambda}\int_0^1 \frac{\mathrm{d}}{\mathrm{d}z}\left[sA\left(\frac{\partial S}{\partial z}\right)^{-1}\right]\mathrm{e}^{\mathrm{i}\lambda S}\,\mathrm{d}z. \end{aligned} \quad (27)$$

We see that repeated integration by parts generates an asymptotic expansion of O_2 in powers of $1/\lambda$. Limiting the result to the first term, and setting λ back to 1, we get

$$O_2 = \frac{s(0)}{2\mathrm{i}r_\mathrm{s}^2 k_\mathrm{s}}\mathrm{e}^{\mathrm{i}S(r_\mathrm{s},1)} \quad (28)$$

on using equation (7). Since $S(r_\mathrm{s},1) \simeq 2(\omega\, t_\mathrm{s} + \delta_0)$ (Roxburgh & Vorontsov 2000a), we arrive again at (26).

3 WAVE PACKETS AND THE ACF

Now instead of considering a monochromatic source, we allow the source to emit a single wave packet centred at frequency ω. We now also allow wave reflection from the stellar surface.

Observer 1: the source side. Strong peaks in the observational time string, produced by the direct wave, will arrive at times $2Tk$ after the excitation, with k even. The amplitude of these peaks will drop slowly with k, at least for the first few skips (Paper I). A first weak peak in the time string produced by the wave reflected from the core will be detected at time $2T$ $(k = 1)$. This wave will be reflected back from the surface and arrive again with the same amplitude at time $4T$ $(k = 2)$, simultaneous with the arrival of the direct wave. The weak peaks in the time string produced by reflection will thus come at time $2Tk$ with all positive integer k. In the ACF, the ratio of the amplitude of the $k = 1$ peak (we designate this amplitude as $|F_1|$ to follow the notations of Paper I) to the amplitude of the $k = 2$ peak ($|F_2|$) is given by the ratio of the amplitudes of O_1 and

O_2 in equations (24) and (26):

$$\left|\frac{F_1}{F_2}\right| = \frac{2}{s(0)}\sum_l \Delta\delta_l(-1)^l\left(\frac{2l+1}{4\pi}\right)^{1/2} c_l = 2\frac{\sum_l \Delta\delta_l(-1)^l(2l+1)^{1/2}c_l}{\sum_l(2l+1)^{1/2}c_l}. \quad (29)$$

Observer 2: the far side. Peaks due to the direct wave arrive at times $2Tk$ with k odd, and peaks due to the reflected arrive at $2Tk$ for all positive integer k. The amplitudes of the weak pulses in the observational time string (delivered by the reflected wave only) and of the strong pulses (delivered by the refracted wave) are in the same ratio, given by the right-hand side of the equation (29). Weak and strong pulses in the time string alternate with each other; the ratio of the $k = 1$ and 2 signals in the ACF measured by Observer 2 is thus the same as when the ACF is measured by Observer 1.

Equation (29) will lose its accuracy, however, if the angular position of the observer does not coincide with z-axis (or for a given observer, the source is displaced from the disc centre, or from the opposite point at the far side of the star). The result of a similar analysis but without a reflected wave (Paper I) is not affected by such a displacement, since the amplitudes of the $k =$ even and the $k =$ odd peaks in the time string will both decrease in the same proportion. The reflected wave, however, is composed of spherical harmonic components of lowest l only and the displacement of the source position will not make the reflected signal smaller. Therefore, we expect equation (29) to provide a result which is somewhat underestimated, within about a factor of 2. We can expect better accuracy from an alternative analysis which addresses the displacements of resonant lines in the observational power spectrum.

4 P-MODE EXPANSION

As in Paper I, we employ the Fourier amplitude of the power spectrum, which is the amplitude of the ACF, to eliminate rapid oscillations in the ACF. As in the analysis described above, we discard the small frequency separations of the unperturbed configuration (proportional to D_δ), which now produce a small effect in the result. With proper rescaling, F_k will now designate the contribution to the Fourier amplitude of the power spectrum at time $t = 2Tk$, which comes from neighbouring modes of a single radial order n (four modes, if the sensitivity of the observations is limited essentially to $l = 0, 1, 2, 3$ only). We introduce a_l as the sensitivity coefficients in power,

$$a_l = c_l^2, \quad (30)$$

and assume that mode amplitudes do not depend on l (mode masses are nearly the same at the low degree). At $k = 2$ we get, in leading order,

$$|F_2| = \sum_l a_l. \quad (31)$$

In evaluating $|F_1|$ we notice, from the eigenfrequency equation (6), that a small variation $\Delta\delta_l$ of the phase shift leads to a frequency variation of $-\Delta\delta_l/T = -\Delta\delta_l\Delta\omega/\pi$, where $\Delta\omega$ is the large frequency separation. We notice that the phase of the harmonic function in the Fourier transform at $k = 1$ changes by π when the p-mode frequency changes by $\Delta\omega/2$ (frequency separation between modes of even and odd degree). A variation $\Delta\delta_l$ of the phase shift will thus induce a variation of phase of the contribution of the corresponding mode to the Fourier transform by an amount $-2\Delta\delta_l$, and we get

$$|F_1| = \sum_l (-1)^l a_l \mathrm{e}^{-2\mathrm{i}\Delta\delta_l}. \quad (32)$$

Linearizing in $\Delta\delta_l$ and using the symmetry relation (17) between the sensitivity coefficients, which is

$$\sum_l (-1)^l a_l = 0, \quad (33)$$

we get

$$|F_1| = -2\mathrm{i}\sum_l \Delta\delta_l(-1)^l a_l, \quad (34)$$

and hence

$$\left|\frac{F_1}{F_2}\right| = 2\frac{\sum_l \Delta\delta_l(-1)^l a_l}{\sum_l a_l}. \quad (35)$$

To compare the results predicted by equations (29) and (35), consider a wave reflection from a small core, which distorts the phase shifts at $l = 0$ only (isotropic scattering). Using equation (29), we obtain

$$\left|\frac{F_1}{F_2}\right|_{\mathrm{Eq}(29)} = \frac{\int_0^{\pi/2} s(\theta)\sin\theta\,\mathrm{d}\theta}{s(0)}\Delta\delta_0, \quad (36)$$

while the analysis of frequency shifts gives

$$\left|\frac{F_1}{F_2}\right|_{\mathrm{Eq}(35)} = \frac{\left[\int_0^{\pi/2} s(\theta)\sin\theta\,\mathrm{d}\theta\right]^2}{\int_0^{\pi/2} s^2(\theta)\sin\theta\,\mathrm{d}\theta}\Delta\delta_0. \quad (37)$$

For a simplest sensitivity function $s(\theta) = \cos\theta$, which would account for area projection and correspond to intensity measurements when there is no limb darkening, we obtain

$$\left|\frac{F_1}{F_2}\right|_{\mathrm{Eq}(29)} = \frac{1}{2}\Delta\delta_0, \qquad \left|\frac{F_1}{F_2}\right|_{\mathrm{Eq}(35)} = \frac{3}{4}\Delta\delta_0. \quad (38)$$

The result predicted by equation (29) is thus underestimated by a factor of 2/3. This example allows a simple estimate of the effect, independent of an exact knowledge of the sensitivity coefficient of a whole-disc measurement. The magnitude of the $k = 1$ peak in the ACF measured relative to the $k = 2$ peak is about $\Delta\delta_0$, if the reflection comes from a stellar core of a small size.

5 DISTORTIONS OF THE PHASE SHIFTS

Exact values of δ_l are given by numerical integration of the fourth-order differential equations for radial wavefunctions. Apart from such a direct computation, good numerical accuracy is achieved by using a distorted-wave Born approximation, applied to a second-order equation, which in turn approximates the complete fourth-order problem (Roxburgh & Vorontsov 1994).

An important simplification can be obtained when there is a sharp variation of seismic parameters (on a scale of a wavelength) of moderately small magnitude, which can then be treated as a perturbation to the slowly varying background configuration (Roxburgh & Vorontsov 2001 and references therein). A problem which can be approached in this way is wave reflection created by a rapid density variation at the boundary of a convective core.

The magnitude of the variations $\Delta\delta_l$ in the phase shifts induced by the near-discontinuity in density at the core boundary is $\epsilon/4$, where ϵ is the magnitude of the discontinuity, $\epsilon = (\rho_2 - \rho_1)/\rho$ [which is assumed to be small compared to one in the perturbational analysis (Roxburgh & Vorontsov 2001)]. These variations are modulated according to the phase of the squared radial eigenfunction at the core boundary. When the core is large (several wavelengths), this phase depends principally on the parity of l only, and differs by π between modes of even and odd l. As the core gets smaller, this simple

picture is destroyed, modes of higher degree become insensitive to the perturbation when it is below the inner turning point and, when the core radius is smaller than about a quarter of wavelength, it only affects δ_0.

From these considerations, a simple estimate of the magnitude of the $k = 1$ signal in the ACF, relative to $k = 2$, is $\epsilon/4$, if the core is not smaller than half of the acoustic wavelength.

6 NUMERICAL SIMULATION

We compare two models of a 1.2 $M_\odot$ main-sequence star: a young model with central hydrogen abundance $X_c = 0.50$ and an old model with $X_c = 0.05$. The young model has a convective core with radius of about 3 per cent of stellar radius, but without any substantial variation in density near the core boundary. The old model has a convective core of about 5 per cent of stellar radius, and very strong (40–50 per cent) and very sharp density variation just above the boundary.

The results obtained with the young model are illustrated in Fig. 1, where the upper panel shows the D_δ values calculated from the oscillation frequencies as

$$D_\delta = \frac{\pi}{4l+6}\frac{\omega_{n,l} - \omega_{n-1,l+2}}{\omega_{n+1,l} - \omega_{n,l}}. \tag{39}$$

With $l = 0$ and 1, this expression evaluates D_δ from the small frequency separations of modes with degree 0, 2 and 1, 3. The expression

$$D_\delta = \frac{\pi}{4}\frac{2\omega_{n,0} - \omega_{n,1} - \omega_{n-1,1}}{\omega_{n,1} - \omega_{n-1,1}} \tag{40}$$

estimates the same quantity from frequencies of $l = 0$, 1 modes. The D_δ values collapse to a single slowly varying function of frequency, which indicates that acoustic wave propagation in the deep interior is very nearly classical.

The lower panel of Fig. 1 shows the ACF, represented by the Fourier amplitude of an artificial power spectrum. The power spectrum was generated using modes of degree l from 0 to 3, with sensitivity coefficients equal to those of *SOHO* MDI measurements (Paper I). The envelope of the power spectrum was taken as a smooth $\cos^2$ function of frequency limited to the interval between 1 and 3 mHz (the width of the envelope function at half-power is 1 mHz). Spectral lines were modelled with Lorentzian profiles of uniform 1 μHz linewidth. The ACF reveals all the features of semiclassical wave propagation; the small frequency separations, governed by D_δ, can be measured from the ACF as described in Paper I. The $k = 1$ peak has a negligibly small amplitude.

Similar results but obtained with the model of the old star are shown in Fig. 2. The semiclassical picture of wave propagation in the deep interior is now completely destroyed in all the frequency range. At frequencies below 3 mHz, when the convective core is relatively small compared to the wavelength, the behaviour of the small frequency separations corresponds to their low-frequency behaviour which is common for old stars, whether or not they possess a convective core (Roxburgh & Vorontsov 2004). This behaviour is such that the D_δ values calculated from $l = 0$, 2 and $l = 1$, 3 modes are very nearly the same, while those calculated from $l = 0$, 1 modes are significantly higher. Though an exact mechanism of such a peculiar behaviour is not yet understood, the distortion of classical wave propagation is apparently related with an overall density contrast accumulated in the stellar core as a result of chemical evolution. The amplitude of the signal observable in the reflected wave, relative to that of the forward wave (the ratio between amplitudes of

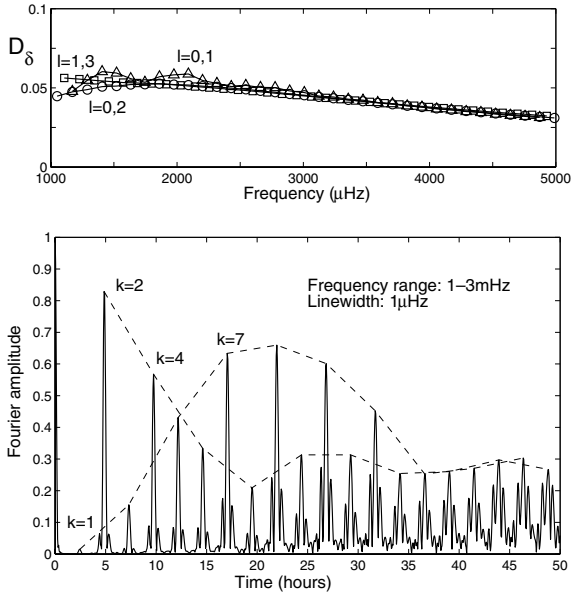

Figure 1. Model of a young 1.2 $M_\odot$ star with central hydrogen abundance $X_c = 0.50$. Top panel: scaled ratio of small to large frequency separations. The D_δ values calculated from frequencies of $l = 0, 2$ modes are shown by the circles and $l = 1, 3$ modes by the squares and $l = 0, 1$ modes by the triangles. Bottom panel: amplitude of Fourier transform of simulated Doppler velocity power spectrum, with frequency range 1–3 mHz and 1 μHz linewidths. We use the Fourier amplitude, which is the envelope of the ACF, to eliminate rapid oscillations in the ACF. The dashed lines connect peaks of the $k =$ even and the $k =$ odd.

$k = 1$ and 2 peaks in the ACF in the middle panel of Fig. 2) is about 5 per cent, at frequencies around 2 mHz.

At frequencies higher than about 3 mHz, the lower turning points of p modes of consecutive degree l start to enter inside the core; the sharp variation of density at the core boundary induces quasi-periodic variations with frequency in the phase shifts and in the small separations. In terms of wave propagation, this is wave reflection from the core boundary. The amplitude of the reflected wave seen at the surface is about 12 per cent of the direct wave (ACF in the bottom panel of Fig. 2). This figure compares well with the simple prediction described in the previous section despite the fact that the magnitude of the density contrast is not small enough to be accurately treated as a perturbation.

To visualize the wave scattering, we numerically simulated a monochromatic wave field produced by a point-like monopole source (Roxburgh & Vorontsov 2000a). The results obtained with the old 1.2 $M_\odot$ star ($X_c = 0.05$) are shown in Fig. 3 at frequencies of 2 and 4 mHz. The excitation source was placed at $r = 0.95R$, and outgoing-wave boundary conditions were imposed at $r = 0.99R$ to eliminate wave reflection from the stellar surface. The simulation was repeated with the same model, but with the equilibrium density profile artificially smoothed in the inner 20 per cent of stellar radius to eliminate its rapid variation; the profile of the adiabatic exponent was retained. In the hydrostatic model, this smoothing also eliminates the corresponding rapid variations in the sound speed and in the buoyancy frequency. By taking the difference between the two wave fields, we can identify the weak-scattered wave.

At 2 mHz frequency the amplitude of the back-scattered wave (upper right panel of Fig. 3) is about 5 per cent of the forward wave (upper left panel), in agreement with measurement made by using the ACF. At 4 mHz, the amplitude of the reflected wave

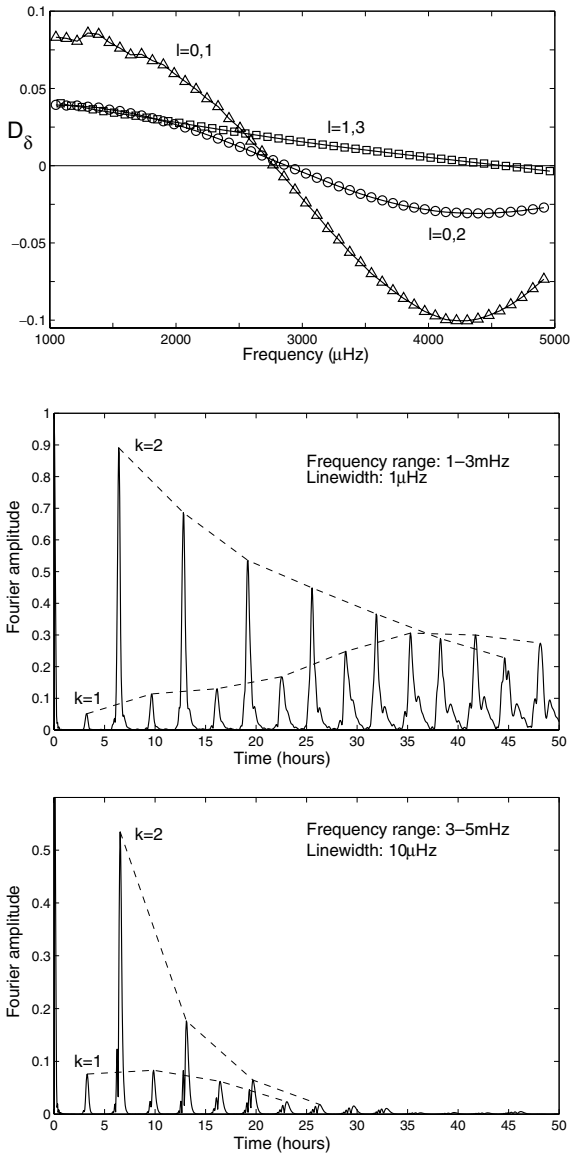

Figure 2. As Fig. 1, but for the model of an old 1.2 $M_\odot$ star with $X_c = 0.05$. Middle panel shows the ACF calculated from the simulated power spectrum limited to the frequency range 1–3 mHz, with 1 μHz linewidths, bottom panel – by the frequency range 3–5 mHz with 10 μHz linewidths.

(lower-right panel), when compared with forward wave (lower-left panel), looks smaller than the result of its measurement with ACF (which is about 12 per cent). The difference is apparently due to the fact that, at higher frequencies, the coherence domain of the forward wave at the surface becomes significantly smaller than the hemisphere, which is the coherence domain of the reflected wave (the scattering is nearly isotropic).

7 DISCUSSION

The magnitude of the observational effect discussed in this paper is relatively small, and prospects of detecting reflected waves in asteroseismic data may be remote. But it is important to have the mechanism of wave reflection understood and the magnitude of the effect quantified. If the $k = 1$ signal in the ACF is detected, it will signify substantial wave reflection coming from the stellar core.

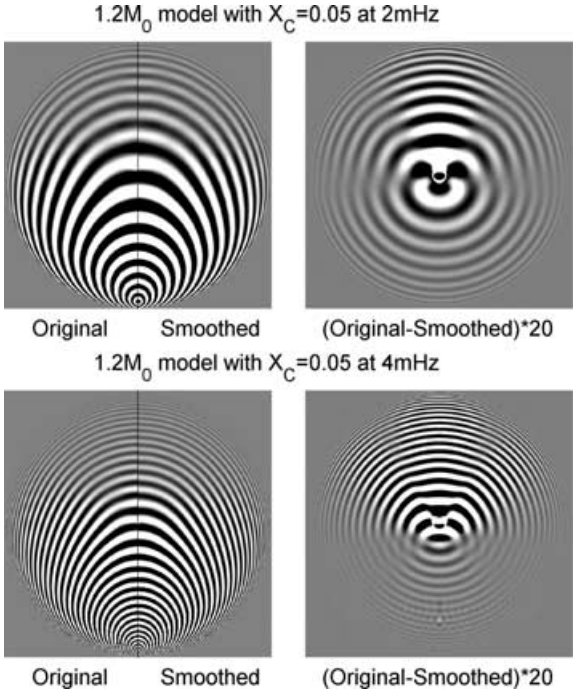

Figure 3. Wave field in the model of an old 1.2 $M_\odot$ star ($X_c = 0.05$) produced by a monochromatic point source. Outgoing-wave boundary conditions were imposed at $r = 0.99$ to eliminate surface reflection. Top panel: frequency 2 mHz; bottom panel: 4 mHz. The panels on the left-hand side show the wave field in the original model, and in the model with the density profile smoothed below $0.2R$ to eliminate wave reflection from the core. The panels on the right-hand side show the differences between the two wave fields, which reveal the scattered wave.

Analysis of the acoustic wave field in three dimensions is a valuable supplement to the traditional normal-mode analysis. It allows us to distinguish which stellar configurations are 'transparent' to acoustic waves, leading to trivial p-mode frequency patterns described by large and small separations, and which are not. How this vision applies to different stars and, in particular, how it can be extended to accommodate possible resonances with internal gravity waves is a matter for further studies.

ACKNOWLEDGMENT

This work was supported by the UK PPARC under grant PPA/G/S/2003/00137.

REFERENCES

Landau L. D., Lifshitz E. M., 1976, Quantum Mechanics. Pergamon Press, Oxford
Roxburgh I. W., Vorontsov S. V., 1994, MNRAS, 267, 297
Roxburgh I. W., Vorontsov S. V., 2000a, MNRAS, 317, 141
Roxburgh I. W., Vorontsov S. V., 2000b, MNRAS, 317, 151
Roxburgh I. W., Vorontsov S. V., 2001, MNRAS, 322, 85
Roxburgh I. W., Vorontsov S. V., 2004, in Favata F., Aigrain S., eds, ESA SP-538, Stellar Structure and Habitable Planet Finding, ESA, Noordwijk, p. 403
Roxburgh I. W., Vorontsov S. V., 2006, MNRAS, 369, 1491 (Paper I)

This paper has been typeset from a TEX/LATEX file prepared by the author.